Tethys: Lithospheric thickness and heat flux from flexurally supported topography at Ithaca Chasma

Bernd Giese,[1] Roland Wagner,[1] Gerhard Neukum,[2] Paul Helfenstein,[3] and Peter C. Thomas[3]

Received 25 July 2007; revised 14 September 2007; accepted 4 October 2007; published 7 November 2007.

[1] We have identified flexural uplift along the flanks of Tethys' Ithaca Chasma using Cassini stereo-derived topography. Modeling the topography as a broken elastic plate yields an effective elastic lithospheric thickness in the range of 5–7 km and, combined with the strength envelope of the lithosphere, a mechanical lithospheric thickness of 16–20 km. Surface heat fluxes are 18–30 mW/m^2 for adopted strain rates of 10^{-17}–10^{-14} s^{-1}. These heat fluxes are more than 4 times higher than those calculated from thermal history models of Tethys and indicate a strongly enhanced local heat flux associated with the formation of Ithaca Chasma. We use crater-size frequency counts and a lunar-like impact chronology to fix the time of formation of Ithaca Chasma at 4 Ga from present-day. Ithaca Chasma predates the Odysseus basin and thus could not have been formed by this impact feature. **Citation:** Giese, B., R. Wagner, G. Neukum, P. Helfenstein, and P. C. Thomas (2007), Tethys: Lithospheric thickness and heat flux from flexurally supported topography at Ithaca Chasma, *Geophys. Res. Lett.*, *34*, L21203, doi:10.1029/2007GL031467.

1. Introduction

[2] Lithospheric thickness and heat flux are indicative of the thermal state of a planetary body and thus provide important constraints on thermal evolution models. Estimates of these parameters can be obtained by analyzing flexurally supported topography like that seen along rifts on Earth [*Weissel and Karner*, 1989] and even on the icy surface of Ganymede [*Nimmo et al.*, 2002]. The shape of the flexed topography allows modeling the effective elastic thickness of the lithosphere and, together with an assumed lithospheric strength envelope, provides estimates of its mechanical thickness and the heat flux. This approach has been used to infer heat fluxes on Ganymede [*Nimmo and Pappalardo*, 2004], Europa [*Ruiz*, 2005], and on Mars [*Grott et al.*, 2005; *Ruiz et al.*, 2006].

[3] In this paper, we utilize Cassini stereo-derived topography of Tethys' Ithaca Chasma to identify features of apparent flexural origin, and use them to obtain estimates of lithospheric thickness and heat flux. In addition, we perform crater size-frequency counts to determine the time of formation of Ithaca Chasma and with it the time to which these estimates apply. We also determine the age of surrounding geological units, in particular the age of the Odysseus impact basin to test whether this basin can account for the formation of Ithaca Chasma as suggested by *Smith et al.* [1981] from Voyager-based studies.

[4] Ithaca Chasma is a prominent feature on Tethys (mean radius ~530 km) first seen in Voyager 1 images [*Smith et al.*, 1981]. It appears as a branching terraced trough about 1000 km long and 50 to 100 km wide. From photoclinometric measurements an average depth of ~3 km was inferred, and a ~0.5 km high raised rim was identified [*Smith et al.*, 1981]. The origin of the trough is controversial. *Smith et al.* [1982] suggested that it formed by freeze-expansion of Tethys' interior or alternatively, that its formation is related to the 400 km Odysseus impact. The latter hypothesis is based on the observation that Ithaca Chasma is confined within a great circle that is roughly concentric with Odysseus [see also *Moore and Ahern*, 1983; *Moore et al.*, 2004].

2. Observations

[5] We study a region across Ithaca Chasma imaged by the ISS Narrow Angle Camera (NAC) during Cassini's 4th and 15th orbits. Figure 1 shows a Digital Elevation Model (DEM) of this region that we derived using stereogrammetric methods [*Giese et al.*, 1998]. It reveals that the chasma transitions from a single, ~100 km wide trunk in the northern section to two narrower branches in the south. Depths reach 2–3 km with respect to the surroundings. Subparallel ridges and troughs inside form terraced walls. The scarps are sharply edged and have a morphology consistent with formation by extensional faulting. The flanks of the chasma are upraised by up to 6 km above the surroundings (Figure 1, p1–p3), significantly higher than Voyager estimates. The overall extensional nature of the chasma and the concave shape of its flanks suggest that the topography arose from flexure.

3. Theory and Methods

[6] To estimate the lithospheric thickness, we treat the lithosphere as a broken elastic plate. First, we determine the effective elastic thickness of the lithosphere by modeling the shape of the flexed plate, and then we relate the effective thickness and the curvature of the plate to the strength envelope of the lithosphere. This yields both the (mechanical) lithospheric thickness and also the heat flux.

[1] German Aerospace Center (DLR), Institute of Planetary Research, Berlin, Germany.
[2] Institute of Geological Sciences, Freie Universität Berlin, Berlin, Germany.
[3] Center for Radiophysics and Space Research, Cornell University, Ithaca, New York, USA.

0094-8276/07/2007GL031467$05.00

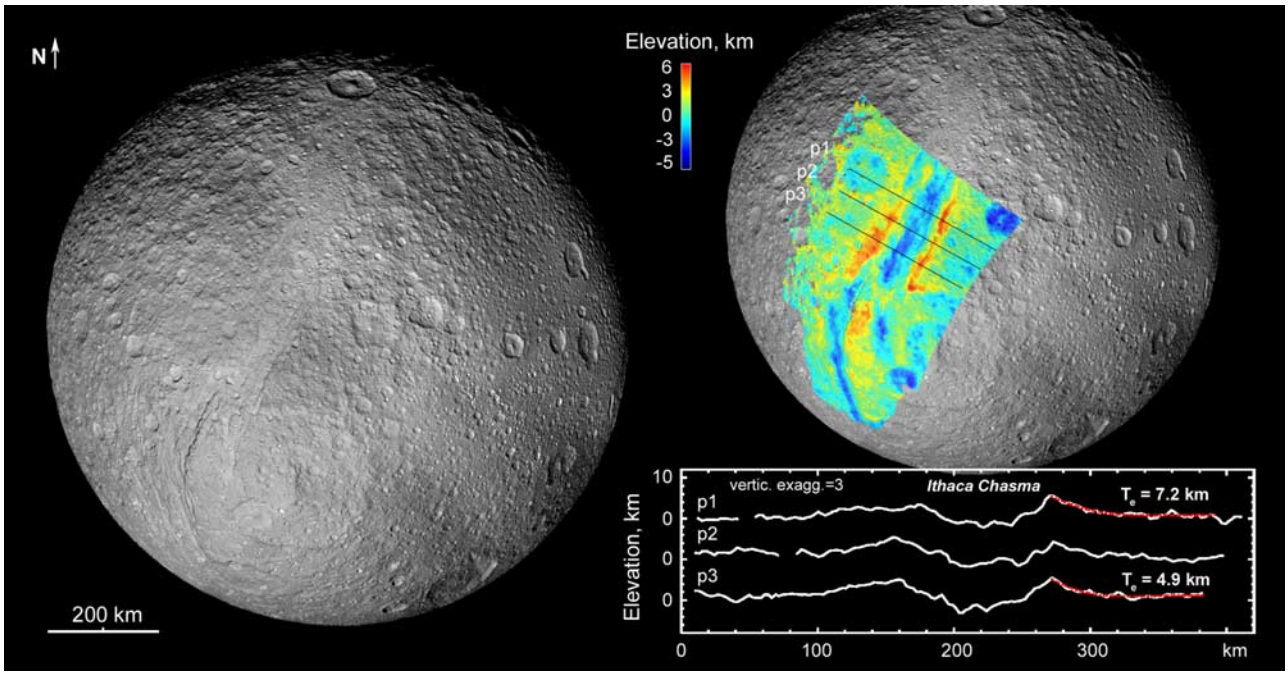

Figure 1. Color-coded DEM across Ithaca Chasma derived from Cassini stereo images (N1489061272, N1489062260; N1506215772, N1506220229, N1506219094, N1506220392) merged with a 400 m/pxl image mosaic centered at 2°S, 16°E. Horizontal resolution is 2–5 km and vertical accuracies range from 150–800 m. The DEM measures local relief only and is not controlled with respect to Tethys' center of figure. The profiles show superimposed (in red) model flexural profiles (Section 5).

[7] The deflection w of a broken elastic plate under a line load is given by [*Turcotte and Schubert*, 2002]

$$w = w_0 e^{-(x/\alpha)} \cos(x/\alpha), \tag{1}$$

where w_0 is the maximum amplitude of deflection, and α is the flexural parameter given by

$$\alpha = \left(\frac{E \cdot T_e^3}{3 \cdot (1-\nu^2) \cdot \Delta\rho \cdot g} \right)^{\frac{1}{4}}, \tag{2}$$

Here, E is the Young's modulus, T_e is the effective elastic thickness, ν is the Poisson's ratio of the material, g is the gravitational acceleration, and $\Delta\rho$ is the density contrast between the lithosphere and the material above.

[8] The observed deflection of the plate is modeled by using equation (1) with an additional offset parameter. For a given value of α (or T_e) we vary w_0 and the offset parameter to minimize the misfit between this model shape and the observed flexed flank.

[9] To relate T_e to the mechanical thickness T_m and thermal structure of the lithosphere we follow the formalism described by *McNutt* [1984]. It is assumed that except for a core, the upper part of the lithosphere is pervasively fractured such that its strength is governed by sliding friction, but in the lower part strength is limited by ductile flow. Within the core, stresses are assumed to be supported elastically. Applying a balance of bending moments supported by this lithosphere and by a pure elastic plate with thickness T_e, *McNutt* [1984] obtained the equation

$$T_e = \left\{ \frac{12 \cdot (1-\nu^2)}{E \cdot K_{\max}} \int_0^{T_m} \sigma(z) \cdot (z - z_n) dz \right\}^{1/3}, \tag{3}$$

where $\sigma(z)$ is the differential stress at depth z to be taken as the least of the brittle strength, the ductile strength, and the fiber stress of the elastic core, and z_n is the depth to the neutral axis at which the fiber stress equals zero (see Figure 2). K is the curvature of the pure elastic plate and must be taken at its maximum [*Mueller and Phillips*, 1995]. T_m is defined via a stress limit σ_b below which contributions to the integral are negligible, and z_n is fixed by the condition that the stress profile integrates to zero. Equation (3) will be used here to determine T_m and the heat flux (see Section 4) at given values of T_e and $K_{\max}$.

4. Constitutive Relations and Strength Parameters

[10] As Tethys's density (see below) is close to that of pure water ice we neglect the impact of any non-water ice components on the ice's strength and flow law here. For the brittle strengths in equation (3) we adopt the relations given by *Beeman et al.* [1988] with a slope of 0.69 and an intercept equal to zero (see Figure 2). The ductile strengths are calculated from the equation

$$\dot{\varepsilon} = \dot{\varepsilon}_1 + \dot{\varepsilon}_2 \tag{4}$$

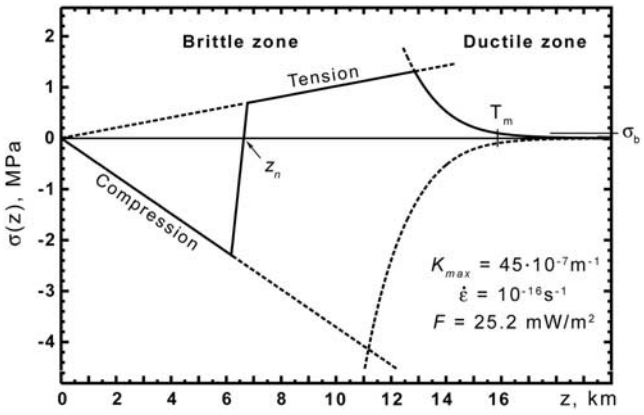

Figure 2. A typical stress profile (solid line) used in equation (3). Brittle and ductile strengths parameters are given in Section 4. For oceanic lithosphere on Earth σ_b is taken at 50 MPa [*McNutt*, 1984], for the icy lithosphere of Tethys we apply a value of 0.1 MPa.

with strain rates $\dot{\varepsilon}_i$ specific to superplastic flow and dislocation creep (basal slip-accommodated grain boundary sliding and diffusion creep turned out to be negligible against these processes) given in the general form by *Ranalli* [1995] and *Goldsby and Kohlstedt* [2001]

$$\dot{\varepsilon} = \left(\frac{\sqrt{3}}{2}\right)^{n+1} \cdot A \cdot \left(\frac{1}{d}\right)^{m} \cdot \sigma(z)^{n} \cdot \exp\left\{-\frac{Q}{R \cdot T(z)}\right\}. \quad (5)$$

Here, d is the grain size, R is the gas constant, and Q is the activation energy (Table 1). For the temperature T(z) at depth z we adopt a conductive profile according to

$$T(z) = T_s \cdot \exp\left\{\frac{F}{567} \cdot z\right\}, \quad (6)$$

where we have used the conductivity of water ice given by *Klinger* [1980]. F is the heat flux in mW/m^2, z is the depth in km, and T_s is the surface temperature.

[11] Throughout the calculations, we adopt $\Delta\rho = 973$ kg/m^3, g = 0.145 m/s^2 [*Thomas et al.*, 2007], $v = 0.33$, $d = 1$ mm, E = 1 GPa, and $T_s = 80$ K.

5. Results

[12] Figures 1 and 3 show the results of fitting the broken elastic plate model to profiles of the eastern flank of Ithaca Chasma. The best fit between the model and the observations is obtained with $T_e = 7.2$ km (p1) and $T_e = 4.9$ km (p3). The maximum curvatures resulting from the model profiles are K_{max}(p1) = 28*10^{-7} m^{-1} and K_{max}(p3) = 45*10^{-7} m^{-1}. For the western flank of Ithaca Chasma a reliable fit is obtained with $T_e = 5.6$ km (p2), which is within the bounds of values determined for the eastern flank. There is significant topography superimposed on the western flank of p1 in particular (evident from Figure 1), which makes this profile inappropriate for elastic thickness estimations.

[13] Using the above bounding values of T_e/K_{max} equation (3) predicts heat fluxes in the range of 23.0–30.0 mW/m^2 and 18.1–23.5 mW/m^2, respectively, for geological strain rates of 10^{-17}–10^{-14} s^{-1} (Figure 4). The grain size dependence of this result is weak. Grain sizes an order of magnitude smaller than adopted (see Section 4) yield heat fluxes smaller by only ~3 mW/m^2 and ~2 mW/m^2, respectively. Also, varying Young's modulus by an order of magnitude changes the solutions by less than 1 mW/m^2.

[14] Mechanical lithospheric thicknesses predicted by equation (3) with T_e = 4.9 km/7.2 km are T_m = 15.8 ± 0.1 km/20.1 ± 0.2 km. The tolerances given here result from a weak dependence on strain rate (10^{-17}–10^{-14} s^{-1}) and grain size (0.1–1 mm). Also, the dependence on the adopted stress limit σ_b (see Figure 2) is weak. Halving σ_b raises T_m by less than 1 km.

6. Ages

[15] Crater size-frequency measurements were performed inside of Ithaca Chasma, outside in the cratered plains, and on the floor of the Odysseus basin (Figure 5). We find a stratigraphic sequence with the cratered plains being the oldest units and Ithaca Chasma being younger, in agreement with previous Voyager-based measurements [*Plescia and Boyce*, 1985]. The Odysseus basin, however, represents the youngest unit. Within a lunar-like impact chronology model [*Neukum*, 1985; *Plescia and Boyce*, 1985; *Neukum et al.*, 2005], Odysseus has an absolute age of 3.9 Ga, the interior of Ithaca Chasma is 4.0 Ga old, and the surrounding cratered plains are 4.1 Ga old (here, a systematic error of ~0.1 Ga resulting from a factor of 2 uncertainty in the impact rate must be applied). Within the impact chronology model of *Zahnle et al.* [2003], absolute ages are much smaller and range from 0.2–1.9 Ga (Odysseus), 0.4–3.3 Ga (interior of Ithaca Chasma), and 0.7–4.3 Ga (cratered plains), respectively. Here, a factor of 3 uncertainty in the impact rate [*Zahnle et al.*, 2003] is used.

7. Discussion and Conclusions

[16] Precise strain rates for Ithaca Chasma are unknown but a potential range can be localized on the basis of the measured extension (see Appendix A). The extension is approximately the product of the strain rate, the (original) feature width (= measured width − extension), and the time span of formation. Assuming that the time span was not shorter than some 0.1 Ma and not longer than some 100 Ma (note that within lunar-like impact chronology models Ithaca Chasma already formed ~500 Ma after Tethys' formation) the range of strain rates is limited to ~10^{-17}–10^{-14} s^{-1}.

Table 1. Rheologic Parameters Used in the Calculations[a]

Creep Process	n	m	Q, [kJ/mol]	A, [MPa^{-n} m^m s^{-1}]
Superplastic flow	1.8	1.4	49	3.9×10^{-3}
Dislocation creep	4	0	60	4×10^{5}

[a]After *Goldsby and Kohlstedt* [2001].

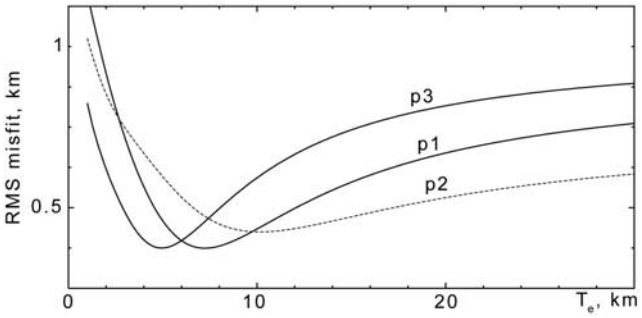

Figure 3. RMS misfit between the model shapes (equation (1)) and observed profiles at the eastern flank of Ithaca Chasma (see Figure 1) in dependence on T_e. Profile p2 was omitted because the misfit is poorer and the minimum less pronounced than for p1 and p3.

[17] The derived mechanical lithospheric thickness of 16–20 km and heat flux of 18–30 mW/m^2 represent the local thermal state associated with the formation of Ithaca Chasma. Elsewhere on Tethys in undeformed regions this state might be different. We can compare our heat flux with those resulting from thermal history models of Tethys [*Multhaup and Spohn*, 2006]. Such models apply to the global thermal conditions and do not consider local effects. Under the most favorable constraints these models provide a heat flux (400 Ma after Tethys' formation) of ~4 mW/m^2. This is much less than derived for Ithaca Chasma and indicates a strongly enhanced heat flux associated with its formation. An enhanced heat flux could have been introduced by the source of the rift extension, or it could have arisen with warm ice welling up in the rift zone in response to extensional unloading. The intrusion of warm ice is fundamentally presumed to have caused the uplifted rift flanks, but its possible contribution to elevated heat flux remains open. We cannot yet exclude the possibility that the predicted strongly enhanced heat flux is a consequence of applying too simple a flexural model to Ithaca Chasma.

[18] The thermal conductivity assumed both here (equation (6)) and by *Multhaup and Spohn* [2006] does not include effects of surface porosity. But porosity on Tethys may be important. *Durham et al.* [2005] have shown that for granulated water ice porosities of 30–40% can be sustained if the pressure is less than 1 MPa (at depths of ~7 km on Tethys). Moreover, fracture porosity is likely to exist across Ithaca Chasma. Porosity lowers the thermal conductivity and would lead to a decreased heat flux. To estimate the impact of porosity we adopted a thermal profile with the conductivity being that of pure water ice (as before) but with an exponential decrease (from a depth z_0) towards the surface according to $exp\{z/z_0 - 1\}$. Using z_0 = 10 km, we found that the heat flux inferred for Ithaca Chasma is reduced by only 34%. Thus, near surface porosity is likely to have a minor impact on the obtained heat fluxes.

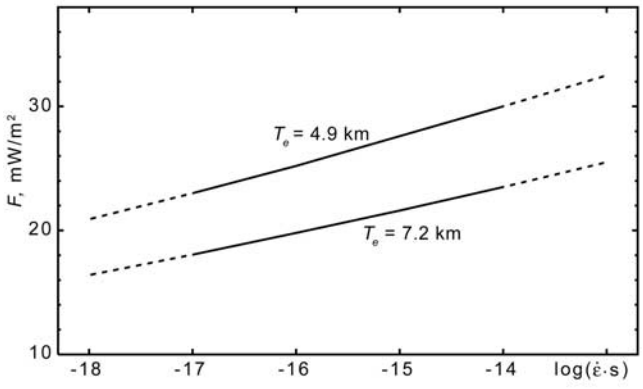

Figure 4. Heat flux as a function of strain rate calculated from equation (3) for different effective elastic thicknesses. Potential strain rates are expected to be in the range of 10^{-17}–10^{-14} s^{-1} (see Section 7).

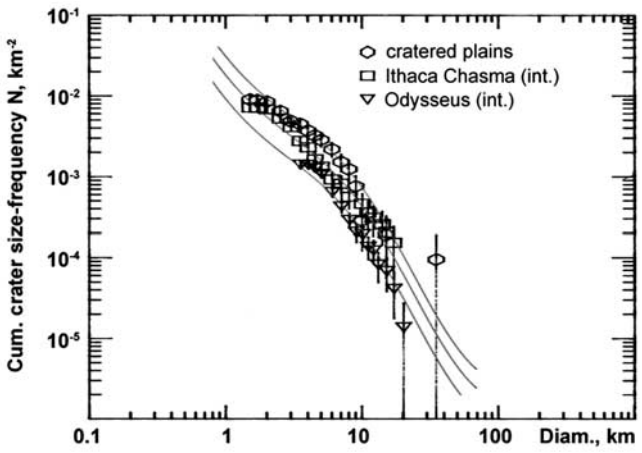

Figure 5. Cumulative crater size-frequency distributions measured in the images. For Odysseus, we used frame N1514129966400 (1.2 km/pxl) taken during Cassini's 19th orbit, otherwise we used the images from Cassini's 15th orbit (Figure 1, left).

[19] The point in time chosen for extracting the heat flux from the thermal history model [*Multhaup and Spohn*, 2006] is about the time of formation of Ithaca Chasma in accordance with the lunar-like impact chronology model. This gives flexurally derived heat fluxes a factor of 6 (for an average heat flux of 24 mWm^{-2}) higher than predicted by thermal modeling. When the *Zahnle et al.* [2003] model is used, however, this factor is in the range of 37–270, which seems to be unrealistically high. On this basis, we suggest that a lunar-like impact chronology model is preferable for determining the age of Tethys and the Saturnian satellites in general.

[20] Our measurements show a higher crater size-frequency on the floor of Ithaca Chasma compared to Odysseus, but we note that this result does not immediately imply an older age for the trough: pre-existing craters on the floor of the chasm may have been passively carried down by (and thus pre-date) the tectonic movements. However, the image data reveal that the interior of Ithaca Chasma was tectonically resurfaced, and a younger crater distribution formed at all measured crater sizes. Consequently, pre-existing craters inside the chasm have been erased which lets us conclude that Odysseus is indeed younger than Ithaca Chasma. Earlier models that attribute its formation to the Odysseus impact are thus incorrect. But also the freeze-expansion

model cannot readily explain how Ithaca Chasma formed [*Smith et al.*, 1982]. This question remains open.

Appendix A

[21] The cumulative extension e_T along a profile is given by $e_T = D_{cum}/tan\ \beta$, where D_{cum} is the cumulative vertical offset of faults and β denotes the fault dip. The strain ε is determined from the length of the profile after extension (L_{final}) and the length of the profile before extension ($l_0 = L_{final} - e_T$) providing $\varepsilon = (L_{final} - l_0)/l_0$. Assuming normal faulting with a fault dip β of 59.4° [*Beeman et al.*, 1988], the cumulative extensions predicted from the measured profiles (Figure 1, p1–p3) are 8–10 km and the strains determined from these are 8–10%.

References

Beeman, M., W. B. Durham, and S. H. Kirby (1988), Friction of ice, *J. Geophys. Res.*, *93*, 7625–7633.

Durham, W. B., W. B. McKinnon, and L. A. Stern (2005), Cold compaction of water ice, *Geophys. Res. Lett.*, *32*, L18202, doi:10.1029/2005GL023484.

Giese, B., J. Oberst, T. Roatsch, G. Neukum, J. W. Head, and R. T. Pappalardo (1998), The local topography of Uruk Sulcus and Galileo Regio obtained from stereo images, *Icarus*, *135*, 303–316.

Goldsby, D. L., and D. L. Kohlstedt (2001), Superplastic deformation of ice: Experimental observations, *J. Geophys. Res.*, *106*, 11,017–11,030.

Grott, M., E. Hauber, S. C. Werner, P. Kronberg, and G. Neukum (2005), High heat flux on ancient Mars: Evidence from rift flank uplift at Coracis Fossae, *Geophys. Res. Lett.*, *32*, L21201, doi:10.1029/2005GL023894.

Klinger, J. (1980), Influence of a phase transition of ice on the heat and mass balance of comets, *Science*, *209*, 271–272.

McNutt, M. K. (1984), Lithospheric flexure and thermal anomalies, *J. Geophys. Res.*, *89*, 11,180–11,194.

Moore, J. M., and J. L. Ahern (1983), The geology of Tethys, *J. Geophys. Res.*, *88*, 577–584.

Moore, J. M., P. M. Schenk, L. S. Bruesch, E. Asphaug, and W. B. McKinnon (2004), Large impact features on middle-sized icy satellites, *Icarus*, *171*, 421–443.

Mueller, S., and R. J. Phillips (1995), On the reliability of lithospheric constraints derived from models of outer-rise flexure, *Geophys. J. Int.*, *123*, 887–902.

Multhaup, K., and T. Spohn (2006), Stagnant lid convection in the mid-sized icy satellites of Saturn, *Icarus*, *186*, 420–435, doi:10.1016/j.icarus.2006.09.001.

Neukum, G. (1985), Cratering records of the satellites of Jupiter and Saturn, *Adv. Space Res.*, *5*(8), 107–116.

Neukum, G., R. Wagner, T. Denk, C. C. Porco, and Cassini ISS Team (2005), The cratering record of the major Saturnian satellites in comparison: First results from analysis of the Cassini ISS imaging data, *Geophys. Res. Abstr.*, *7*, Abstract EGU05-A-07563.

Nimmo, F., and R. T. Pappalardo (2004), Furrow flexure and ancient heat flux on Ganymede, *Geophys. Res. Lett.*, *31*, L19701, doi:10.1029/2004GL020763.

Nimmo, F., R. T. Pappalardo, and B. Giese (2002), Effective elastic thickness and heat flux estimates on Ganymede, *Geophys. Res. Lett.*, *29*(7), 1158, doi:10.1029/2001GL013976.

Plescia, J. B., and J. M. Boyce (1985), Impact cratering history of the Saturnian satellites, *J. Geophys. Res.*, *90*, 2029–2037.

Ranalli, G. (1995), *Rheology of the Earth*, 2nd ed., Chapman and Hall, London.

Ruiz, J. (2005), The heat flow of Europa, *Icarus*, *177*, 438–446.

Ruiz, J., P. J. McGovern, and R. Tejero (2006), The early thermal and magnetic state of the cratered highlands of Mars, *Earth Planet. Sci. Lett.*, *241*, 2–10, doi:10.1016/j.epsl.2005.10.016.

Smith, B. A., et al. (1981), Encounter with Saturn: Voyager 1 imaging science results, *Science*, *212*, 163–191.

Smith, B. A., et al. (1982), A new look at the Saturn system: The Voyager 2 images, *Science*, *215*, 504–537.

Thomas, P. C., et al. (2007), Shapes of the Saturnian icy satellites and their significance, *Icarus*, *190*, 573–584, doi:10.1016/j.icarus.2007.03.012.

Turcotte, D. L., and G. Schubert (2002), *Geodynamics*, 2nd ed., Cambridge Univ. Press, Cambridge.

Weissel, J. K., and G. D. Karner (1989), Flexural uplift of rift flanks due to mechanical unloading of the lithosphere during extension, *J. Geophys. Res.*, *94*, 13,919–13,950.

Zahnle, K., P. Schenk, H. Levison, and L. Dones (2003), Cratering rates in the outer Solar System, *Icarus*, *163*, 263–289.

B. Giese and R. Wagner, DLR-Institut für Planetenforschung, Rutherfordstraße 2, 12489 Berlin, Germany. (bernd.giese@dlr.de)

P. Helfenstein and P. C. Thomas, Center for Radiophysics and Space Research, Cornell University, Ithaca, NY 14853, USA.

G. Neukum, Institut für Geologische Wissenschaften, Freie Universität Berlin, 12249 Berlin, Germany.